Article

# Functionalization of Zeolitic Cavities: Grafting NH Groups in Framework T Sites of B-SSZ-13 A Way to Obtain Basic Solids Catalysts?

Laura Regli, Silvia Bordiga, Claudia Busco, Carmelo Prestipino, Piero Ugliengo, Adriano Zecchina, and Carlo Lamberti

*J. Am. Chem. Soc.*, **2007**, 129 (40), 12131-12140• DOI: 10.1021/ja0721770 • Publication Date (Web): 15 September 2007



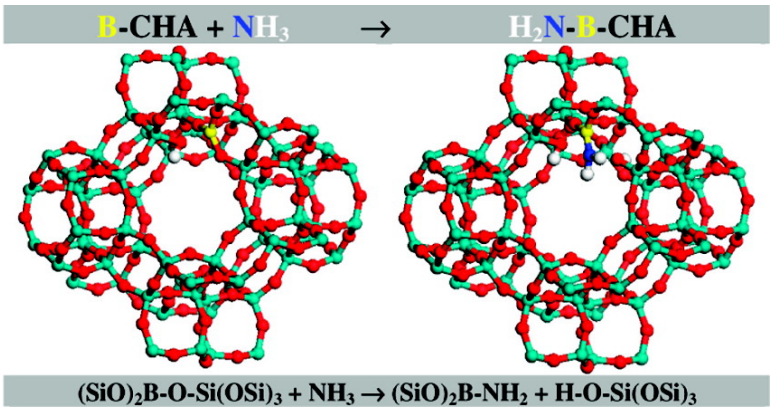

J|A|C|S
ARTICLES
Published on Web 09/15/2007

# Functionalization of Zeolitic Cavities: Grafting $NH_2$ Groups in Framework T Sites of B-SSZ-13 — A Way to Obtain Basic Solids Catalysts?

Laura Regli,[†] Silvia Bordiga,*[,†] Claudia Busco,[‡] Carmelo Prestipino,[§] Piero Ugliengo,[†] Adriano Zecchina,[†] and Carlo Lamberti[†]

*Contribution from the Department of Inorganic, Physical and Materials Chemistry, NIS Centre of Excellence, and Centro di Riferimento INSTM, University of Turin, Via P. Giuria 7, I-10125, Torino, Italy, DiSCAFF and NIS Centre of Excellence, Via Bovio 6, 28100 Novara, Italy, and ESRF, 6 rue Jules Horowitz, BP220, F-38043, Grenoble CEDEX, France*

Received March 28, 2007; E-mail: silvia.bordiga@unito.it

***Abstract:*** Insertion of B atoms into an Al-free zeolitic framework with CHA topology results in the formation of B-SSZ-13 zeotype with Si/B = 11. B K-edge NEXAFS testifies that B forms $[B(OSi)_4]$ units in a $T_d$-like geometry ($sp^3$-hybridized B atoms). According to B K-edge NEXAFS and IR, template burning results in the formation of $[B(OSi)_3]$ units in a $D_{3h}$-like geometry ($sp^2$-hybridized B atoms) with a break of a B−O−Si bond and the formation of a Si−OH group. The activated material contains B(III) Lewis acid centers able to specifically coordinate bases like $NH_3$. Such $[B(OSi)_3]$ units are reactive toward ammonia, resulting in the formation of B−$NH_2$ surface functionality inside the pores of B-SSZ-13 already under mild conditions, i.e., 35 mbar of $NH_3$ at 373 K for 30 min and without crystallinity degradation. A minor fraction of Si−$NH_2$ cannot be excluded owing to the presence of two IR doublets at 3500 and 3430 $cm^{-1}$ and at 1600 and 1550 $cm^{-1}$. *Ab initio* B3LYP/6-31+G(d,p) calculations on a cluster model, supported by a single-point MP2 on B3LYP/6-31+G(D,P) optimized structures, found the break by $NH_3$ of a B−O−Si bond of the $[B(OSi)_3]$ unit with formation of [SiOH] and $[H_2N-B(OSi)_2]$ species to be energetically favored. Comparison between experimental and computed frequency shifts shows them to be in semiquantitative agreement. The high stability of the B−$NH_2$ surface functionality is probed by N K-edge NEXAFS spectra collected under UHV conditions. These findings can open a new route in the preparation of shape selective solid basic catalysts.

## 1. Introduction

Zeolites are well-known as acid catalysts, due to the presence of Brønsted and Lewis sites associated with framework $Al^{3+}$ species.[1−8] However, more recently, the need of basic solids for replacement liquid bases in industrial processes[9,10] has stimulated more extensive research toward zeolites with basic properties.[11] In this sense, alkaline exchanged and overexchanged zeolites[12,13] have been used successfully together with sepiolites,[14] alkaline earth oxides,[15] hydrotalcites,[16] resins,[17] and alkaline earthcarbonates.[18] The basicity in alkaline exchanged and overexchanged zeolites is of Lewis type, and it is associated with framework oxygens. The basicity strength increases with decreasing charge-to-radius ratio of the alkaline counterion. Similarly, alkali-oxide clusters encaged inside zeolites have been also considered.[9,10] The obtained materials are however bases of low strength, limiting their applicability in organic syntheses; but they can be handled in air, since the "base sites" are resistant to poisoning of water or carbon dioxide.[10] Conversely, encapsulation of alkali-metal clusters and amide impregnated zeolites give rise to materials sensitive to contact with air or moisture. A completely different approach to obtain basic solids has been considered by substitution of some framework oxygens by $NH_x$ groups. An extensive nitridation of amorphous silica,[19] amorphous aluminophospates,[20] mesoporous silica,[21] zeolites,[22] and

[†] University of Turin.
[‡] DiSCAFF and NIS Centre of Excellence.
[§] ESRF.

(1) Liu, Z. M.; Liang, J. *Curr. Opin. Solid State Mater. Sci.* **1999**, *4*, 80−84.
(2) Stocker, M. *Microporous Mesoporous Mater.* **1999**, *29*, 3−48.
(3) Sato, H. *Catal. Rev.—Sci. Eng.* **1997**, *39*, 395−424.
(4) Armor, J. N.; Toby, B. H. Zeolites offer variety as ligands; *Electron Transfer Reactions*; American Chemical Society: Washington, DC, 1997; Vol. 253, pp 91−98.
(5) Corma, A. *Curr. Opin. Solid State Mater. Sci.* **1997**, *2*, 63−75.
(6) Zecchina, A.; Otero Arean, C. *Chem. Soc. Rev.* **1996**, *25*, 187−197.
(7) Farneth, W. E.; Gorte, R. J. *Chem. Rev.* **1995**, *95*, 615−635.
(8) Bjorgen, M.; Bonino, F.; Kolboe, S.; Lillerud, K. P.; Zecchina, A.; Bordiga, S. *J. Am. Chem. Soc.* **2003**, *125*, 15863−15868.
(9) Hattori, H. *Chem. Rev.* **1995**, *95*, 537−558.
(10) Barthomeuf, D. *Catal. Rev.—Sci. Eng.* **1996**, *38*, 521−612.
(11) Weitkamp, J.; Hunger, M.; Rymsa, U. *Microporous Mesoporous Mater.* **2001**, *48*, 255−270.
(12) Corma, A.; Fornes, V.; Martinaranda, R. M.; Garcia, H.; Primo, J. *Appl. Catal.* **1990**, *59*, 237−248.
(13) Rodriguez, I.; Cambon, H.; Brunel, D.; Lasperas, M.; Geneste, P. *Stud. Surf. Sci. Catal.* **1993**, *78*, 623−630.
(14) Corma, A.; Martinaranda, R. M. *J. Catal.* **1991**, *130*, 130−137.
(15) Moison, H.; Texier-Boullet, F.; Foucaud, A. *Tetrahedron* **1987**, *43*, 537−542.
(16) Corma, A.; Fornes, V.; Martinaranda, R. M.; Rey, F. *J. Catal.* **1992**, *134*, 58−65.
(17) Tanabe, K. In *Catalysis by Acids and Bases*; Imelik, B., Ed.; Elsevier: Amsterdam, 1985; p 1.
(18) Aramendia, M. A.; Borau, V.; Jimenez, C.; Marinas, J. M.; Romero, F. J. *Chem. Lett.* **1995**, 279−280.
(19) Folman, M. *Trans. Faraday Soc.* **1961**, *57*, 2000−2006.

crystalline aluminophosphates (ALPOS)[23−26] requires prolonged treatments (many hours or days) in an $NH_3$ atmosphere at high temperature (700−1100 K). The nitrogen content of the oxynitrides (proportionally related with the basicity of the solid) can be varied with the time and temperature of nitridation; in any case, the nitridation procedure causes structural damage due to the prolonged ammonia treatment at high temperatures.

Hence, alternative methods able to introduce $NH_x$ species under milder conditions, e.g., using either more active nitridation reagents or dopants which catalyze the partial decomposition of ammonia into more reactive nitridation species, would be very interesting. The latter was recently described by Xiong et al.[27] who reported that Ru-modified silicoaluminophosphates can be nitridated already at temperatures around 673 K, since ammonia is decomposed into more reactive species on the noble metal. Very recently Avenier et al.[28] report the formation at room temperature of $-NH_2$ species on silica- and MCM-41-supported siloxy tantalum hydrides.

Nitridates zeolites and zeotypes have shown catalytic properties in Knoevenagel condensation of benzaldehyde with active methylene compounds.[22,25] Furthermore, the functionalization of microporous materials with $NH_x$ species could be also of interest as metal ion sensors.[29]

A new strategy to easily prepare nitridated zeolites, under very mild conditions (35 mbar, 1 h at 373 K), without crystallinity degradation, is described in this work, where the reactivity toward $NH_3$ of a boron-substituted B-SSZ-13 (a high silica zeolite with CHA framework) has been investigated by a combined use of vibrational spectroscopy and near edge X-ray absorption fine structure spectroscopy (NEXAFS), in the soft X-ray region. Experimental data have been supported by *ab initio* calculations. It will be shown the role played by boron present in substitutional positions in the activation of the framework allowing the easy insertion of $NH_x$ species. A similar reactivity has been recently observed also in the case of $CH_3$-OH, where an extensive methoxylation has been observed at room temperature.[30]

## 2. Experimental Section

**2.1. Synthesis of B-SSZ-13 and Nitridation Procedure.** *N,N,N*-Trimethyl-1-adamantammonium hydroxide (106 mmol), in 175 mL of water, is used to dissolve 2.15 g of Boric acid (∼35 mmol). After the solution is clear, 26.13 g of Carbosil M-5 (97% $SiO_2$, remainder $H_2O$) are added in with stirring. The reactants have been mixed in the Teflon liner for a 600 $cm^3$ Parr overhead stirrer reactor. The reactor is closed up, and while being stirred at 75 RPM, it is ramped to 433 K over an 8 h period. The reaction is held at this temperature for 3 more days. An analysis of the settled reaction product shows it to be a borosilicate Chabazite (hereafter B-SSZ-13) pattern with some symmetry differences from the usual aluminosilicate material. The material obtained shows a Si/B ratio of 11, which implies one heteroatom per unit cell and an average of one B(III) species in any cage. This composition is the most favorable when a big template (*N,N,N*-trimethyl-1-adamantammonium hydroxide) is used, because any template molecule is neutralized by B(III) species. The purity of the compound is testified by the absence of reflections not belonging to the CHA structure in the XRPD pattern collected at the GILDA BM8 beamline at the ESRF synchrotron,[30] equipped with a flat Fuji 200 × 400 $mm^2$ image plate (IP) supported by a magnetic plate.[31,32]

Nitridated B-SSZ-13 zeolite has been obtained by contacting the calcined sample with $NH_3$ (equilibrium pressure 35 mbar) for 1 h at 373 K. This very mild treatment prevents the crystallinity degradation of the zeolite as testified by XRD and BET experiments. In particular, XRD patterns collected before and after nitridation are very similar; compare black and gray curves in Figure S1 of the Supporting Information. Le Bail refinement,[33] in the $R\bar{3}m$ space group,[34] resulted in almost unaffected lattice parameters and cell angles. The as-calcined B-SSZ-13 resulted in $a = b = c = 9.1892(3)$ Å, $\alpha = \beta = \gamma = 94.323(1)°$, and $V = 768.96(4)$ $Å^3$, while for the $NH_3$-treated one we obtained $a = b = c = 9.1905(6)$ Å, $\alpha = \beta = \gamma = 94.228(2)°$, and $V = 769.61(9)$ $Å^3$. The quality of the refinement can be appreciated in Figure S2 of the Supporting Information. BET experiments indicate that the surface area decreases slightly from 890 $m^2/g$ down to 760 $m^2/g$, after the treatment in ammonia.

**2.2. Characterization Techniques and ab Initio Methods.** B and N K-edge NEXAFS spectra have been collected at the BEAR beamline of the ELETTRA synchrotron (Trieste, Italy) equipped with a plane grating monochromator.[35] The acquisition has been made in the total fluorescence yield mode, by the use of a photodiode inside the chamber, at the temperature 100 K. The choice of fluorescence detection was driven by the isolating nature of the materials that strongly affect the quality of spectra recorded by electron base detection (TEY, PEY...). The zeolite samples were mounted on the standard VG Scienta "VG XL25" sample holder, when necessary thermal treated in the preparation chamber, and finally inserted in the experimental station of the beamline for the measurement (residual pressure lower than $10^{-9}$ mbar). Data were recorded with a sampling step of 0.1 eV with a sampling count of 2 s/point. For each sample, a number ranging between five and eight successive spectra (depending on the statistic) was reordered in the same experimental condition and averaged *a posteriori*. As references for boron atoms in tetrahedral or trigonal planar geometries, $BPO_4$ and $B_2O_3$ model compounds have been reported.[36,37] Data have been collected on the same beamline by Prof. F. Boscherini.[38]

NEXAFS spectra have been collected on as-synthesized, calcined, and nitridated (after interaction with $NH_3$ at 373 K) B-SSZ-13. Calcination and interaction with ammonia have occurred ex situ before insertion in the BEAR prechamber. We have observed that the B K-edge spectra of as-synthesized B-SSZ-13 collected at room temperature was not stable, progressively evolving to that measured on the calcined


(20) Grange, P.; Bastians, P.; Conanec, R.; Marchand, R.; Laurent, Y. *Appl. Catal., A* **1994**, *114*, L191−L196.
(21) Xia, Y. D.; Mokaya, R. *Angew. Chem., Int. Ed.* **2003**, *42*, 2639−2644.
(22) Narasimharao, K.; Hartmann, M.; Thiel, H. H.; Ernst, S. *Microporous Mesoporous Mater.* **2006**, *90*, 377−383.
(23) Stein, A.; Wehrle, B.; Jansen, M. *Zeolites* **1993**, *13*, 291−298.
(24) Wong, H.; Yang, B. L.; Cheng, Y. C. *Appl. Surf. Sci.* **1993**, *72*, 49−54.
(25) Climent, M. J.; Corma, A.; Fornes, V.; Frau, A.; GuilLopez, R.; Iborra, S.; Primo, J. *J. Catal.* **1996**, *163*, 392−398.
(26) Corma, A.; Pedro, V.; Fernandez, L. *J. Mol. Catal. A: Chem.* **1998**, *133*, 241−250.
(27) Xiong, J. M.; Ding, Y. J.; Zhu, H. J.; Yan, L.; Liu, X. M.; Lin, L. W. *J. Phys. Chem. B* **2003**, *107*, 1366−1369.
(28) Avenier, P.; Lesage, A.; Taoufik, M.; Baudouin, A.; De Mallmann, A.; Fiddy, S.; Vautier, M.; Veyre, L.; Basset, J. M.; Emsley, L.; Quadrelli, E. A. *J. Am. Chem. Soc.* **2007**, *129*, 176−186.
(29) Clavier, C. W.; Rodman, D. L.; Sinski, J. F.; Allain, L. R.; Im, H. J.; Yang, Y.; Clark, J. C.; Xue, Z. L. *J. Mater. Chem.* **2005**, *15*, 2356−2361.
(30) Regli, L.; Bordiga, S.; Lamberti, C.; Lillerud, K. P.; Zones, S. I.; Zecchina, A. *J. Phys. Chem. C* **2007**, *111*, 2992−2999.
(31) Meneghini, C.; Artioli, G.; Balerna, A.; Gualtieri, A. F.; Norby, P.; Mobilio, S. *J. Synchrotron Radiat.* **2001**, *8*, 1162−1166.
(32) Milanesio, M.; Artioli, G.; Gualtieri, A. F.; Palin, L.; Lamberti, C. *J. Am. Chem. Soc.* **2003**, *125*, 14549−14558.
(33) Le Bail, A. *Powder Diffr.* **2005**, *20*, 316−326.
(34) Calligaris, M.; Nardin, G.; Randaccio, L. *Zeolites* **1983**, *3*, 205−208.
(35) Nannarone, S.; Borgatti, F.; DeLuisa, A.; Doyle, B. P.; Gazzadi, G. C.; Giglia, A.; Finetti, P.; Mahne, N.; Pasquali, L.; Pedio, M.; Selvaggi, G.; Naletto, G.; Pelizzo, M. G.; Tondello, G. *AIP Conf. Proc.* **2004**, *705*, 450−453.
(36) Schmidt, M.; Ewald, B.; Prots, Y.; Cardoso-Gil, R.; Armbruster, M.; Loa, I.; Zhang, L.; Huang, Y. X.; Schwarz, U.; Kniep, R. *Z. Anorg. Allg. Chem.* **2004**, *630*, 655−662.
(37) Gurr, G. E.; Montgomery, P. W.; Knutson, C. D.; Gorres, B. T. *Acta Crystallogr., Ser. B* **1970**, *26*, 906−915.
(38) Carboni, R.; Pacchioni, G.; Fanciulli, M.; Giglia, A.; Mahne, N.; Pedio, M.; Nannarone, S.; Boscherini, F. *Appl. Phys. Lett.* **2003**, *83*, 4312−4314.

sample. To minimize soft X-ray-induced decomposition of the template molecule, all reported spectra have been collected at liquid nitrogen temperature.

B-SSZ-13 zeolite, after calcination at 773 K in vacuum, has been characterized by FTIR spectroscopy in transmission mode. All IR spectra have been collected at room temperature. The vibrational information relevant in our study lies in two different regions: (i) the 1400−700 $cm^{-1}$ range covering framework modes able to highlight the presence and the nature of B species (tetrahedral-like or trigonal planar); (ii) the 3800−2400 $cm^{-1}$ range representative of Brønsted OH species, either unperturbed or after interaction with probes. As region (i) is dominated by the strong silica modes, an optimum sample thickness able to result in high quality IR spectra on both regions could not be found and IR experiments have been duplicated. To follow in detail the spectral evolution in the 1400−700 $cm^{-1}$ range, a very thin film of B-SSZ-13 has been deposited on a silicon wafer from a water suspension. Conversely, when the attention is turned toward the reactivity of surface species with $NH_3$, a compressed self-supporting zeolite wafer (about 23 $mg/cm^2$) has been used. Both types of experiments have been performed at room temperature adopting a 2 $cm^{-1}$ resolution on a Bruker IFS66 FTIR spectrometer, equipped with an MCT cryo-detector. An ad hoc conceived IR cell has been used, allowing in situ thermal treatments and molecule dosage to be done.[39,40]

The effect of the nitridization treatment on the sample crystallinity has been checked with a Philips PW 1830 instrument equipped with Co Kα radiation ($\lambda = 1.789$ Å). The surface area was obtained by $N_2$ adsorption measurements carried out at 77 K on a Micromeritics ASAP 2020 sorption analyzer.

Molecular modeling has been performed using the Gaussian03 computer code[41] within the DFT approach. Models, based on silica cage clusters,[42−47] have been adopted in order to study the thermochemical process of the B−O−Si bond breaking by $NH_3$ and the relative stability of the resulting $-NH_2$ surface species anchored on B and Si atoms. A hybrid B3LYP/6-31+G(D,P) functional with the standard Gaussian 6-31+G(d,p) basis set has been adopted to fully optimize the considered structures and to compute the harmonic frequencies, which resulted in being all positive for the reported equilibrium structures (minima on the potential energy surface). MP2/6-311++-(2p,2d) single-point energy calculations on the B3LYP/6-31+G(D,P) optimized geometries have been also carried out to improve the evaluation of the energetics of the reactions. The B3LYP/6-31+G-(D,P) energetics of the considered reaction have been computed using enthalpies at 298 K derived by correcting the electronic energies by the zero-point energy and by thermal corrections. For MP2 results only electronic energies are reported owing to the missing set of MP2 frequencies.

## 3. Results and Discussion

B K-edge NEXAFS (section 3.1) and IR (Section 3.4) have been selected as experimental characterization techniques particularly suitable in discriminating between $[B(OSi)_4]$ units in a $T_d$-like geometry ($sp^3$-hybridized B atoms) and $[B(OSi)_3]$ units in a $D_{3h}$-like geometry ($sp^2$-hybridized B atoms). Moreover, the possible nitridation of the zeolitic framework can be easily followed by the specific electronic and vibrational features of $-NH_2$ groups by N K-edge NEXAFS (section 3.2 Experimental Section and section 3.3 Simulation of NEXAFS spectra) and IR (section 3.4) spectra, respectively. Ab initio calculations have been performed on a cage cluster in order to highlight the energetic aspects of two different possible pathways for the nitridation process and to substantiate the IR and NEXAFS data (section 3.5).

**3.1. NEXAFS Study of Template Removal.** B K-edge NEXAFS spectra of B-SSZ-13 in the presence of a template (solid black curve), after calcination (dotted curve) and after interaction with $NH_3$ at 373 K (solid gray curve), are reported in Figure 1a. All the spectra have been normalized imposing that the average intensity in the 210−215 eV region, where they exhibit an almost flat line shape, is equal to a unit.

The spectrum collected in the presence of a template is characterized by three main components at 194.4, 198.5, and 203.0 eV, whose intensities are 1.0, 1.4, and 1.3, respectively. The components at 198.5 and 203.0 eV are due to B in $sp^3$ hybridization as similar features have been observed at similar energies, in the $BO_4$ tetrahedral units of bulk $BPO_4$,[48] (see also the spectrum reported in Figure 1b) while they are slightly shifted at 197.5 and 204.8 eV in bulk c-BN.[49] Similar components have been observed by Carboni et al.[38] on amorphous B−P-silicate, where the presence of P forces B atoms into tetrahedral coordination. In our sample, the relatively broad nature of these bands is attributed to a distortion of $BO_4$ tetrahedra that results in loss of the degeneracy of $\sigma^*(t_2)$ orbitals and consequently broadening of the transitions. The component at 198.5 eV is readily assigned to transition of B 1*s* to antibonding ($\sigma^*$) states: $T_2$ and $A_1$ symmetry of tetrahedral $BO_4$ groups. Regarding the feature at 194.4 eV, it is attributed to the B $1s \rightarrow \pi^*$ resonance, which is associated with $sp^2$ hybridization and planar bonding.[38,49−52] However, in the B-SSZ-13 sample with the template, the fraction of B atoms that exhibits a planar geometry with $sp^2$ hybridization is very low, as the $1s \rightarrow \pi^*$ resonance is very sharp and intense in materials exhibiting only this phase. As an example, its intensity, in spectra normalized in a similar way, is as high as 12 in bulk h-BN or as high as 9 in $sp^2$-hybridized BN nanotubes, where its position occurs at 191.8 eV.[49]

These attributions are confirmed by the NEXAFS spectrum collected on the calcined B-SSZ-13 sample (dotted line in Figure 1a), where both features at 198.5 and 203.0 eV, ascribed due to B in $sp^3$ hybridization, disappear and where the 194.4 eV component dominates the spectrum, having an intensity as high as 8.2 and an FWHM as narrow as 0.55 eV. As a consequence, this component can be defined as the B $sp^2$ fingerprint band in NEXAFS spectra (see the spectrum of $B_2O_3$ model compound in Figure 1c) dominated by a component at 194.2 eV. Besides this dominant component, other minor features characterize the

(39) (a) Zecchina, A.; Scarano, D.; Bordiga, S.; Spoto, G.; Lamberti, C. *Adv. Catal.* **2001**, *46*, 265−397. (b) Lamberti, C.; Groppo, E.; Spoto, G.; Bordiga, S.; Zecchina, A. *Adv. Catal.* **2007**, *51*, 1−74.
(40) Groppo, E.; Lamberti, C.; Bordiga, S.; Spoto, G.; Zecchina, A. *Chem. Rev.* **2005**, *105*, 115−183.
(41) Frisch, M. J., et al. *Gaussian 03*, revision C.02; Wallingford, CT, 2004.
(42) Civalleri, B.; Garrone, E.; Ugliengo, P. *Langmuir* **1999**, *15*, 5829−5835.
(43) Bolis, V.; Busco, C.; Bordiga, S.; Ugliengo, P.; Lamberti, C.; Zecchina, A. *Appl. Surf. Sci.* **2002**, *196*, 56−70.
(44) Garrone, E.; Onida, B.; Bonelli, B.; Busco, C.; Ugliengo, P. *J. Phys. Chem. B* **2006**, *110*, 19087−19092.
(45) Bolis, V.; Busco, C.; Ugliengo, P. *J. Phys. Chem. B* **2006**, *110*, 14849−14859.
(46) Busco, C.; Bolis, V.; Ugliengo, P. *J. Phys. Chem. C* **2007**, *111*, 5561−5567.
(47) Bordiga, S.; Bonino, F.; Damin, A.; Lamberti, C. *Phys. Chem. Chem. Phys.* **2007**, *9*, 4854−4878.
(48) Fleet, M. E.; Muthupari, S. *Am. Miner.* **2000**, *85*, 1009−1021.
(49) Hemraj-Benny, T.; Banerjee, S.; Sambasivan, S.; Fischer, D. A.; Han, W.; Misewichd, J. A.; Wong, S. S. *Phys. Chem. Chem. Phys.* **2005**, *7*, 1103−1106.
(50) Stöhr, J. *NEXAFS spectroscopy*; Springer-Verlag: Berlin, 1992.
(51) Ishiguro, E.; Iwata, S.; Suzuki, Y.; Mikuni, A.; Sasaki, T. *J. Phys. B: At. Mol. Phys.* **1982**, *15*, 1841−1854.
(52) Terminello, L. J.; Chaiken, A.; Lapianosmith, D. A.; Doll, G. L.; Sato, T. *J. Vac. Sci. Technol., A* **1994**, *12*, 2462−2466.

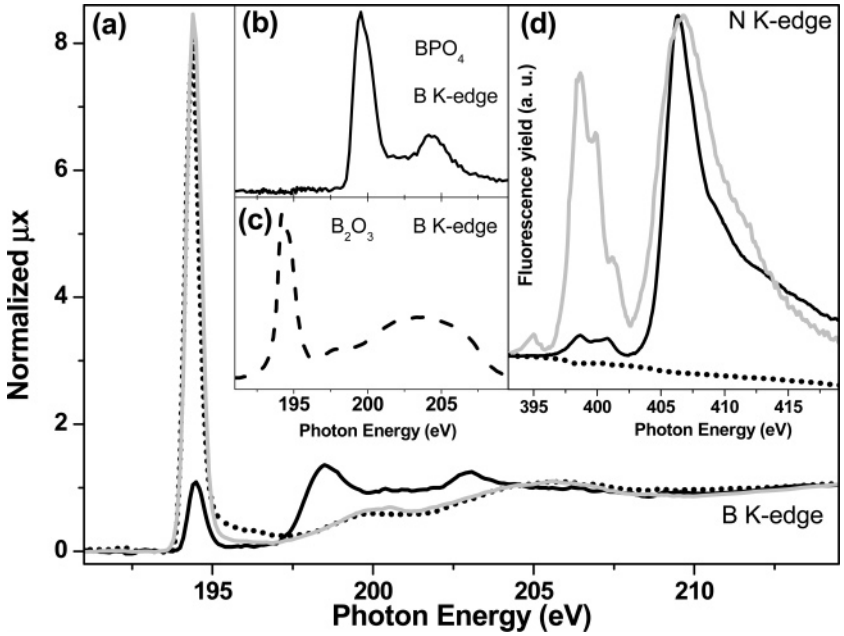


***Figure 1.*** (a) Normalized B K-edge NEXAFS spectra of B-SSZ-13 in presence of template (solid black curve), after calcination (dotted curve), and after interaction with $NH_3$ at 373 K (solid gray curve). (b) NEXAFS spectrum of $BPO_4$ model compound ($sp^3$-hybridized B atoms, $T_d$-like geometry). (c) NEXAFS spectrum of $B_2O_3$ model compound ($sp^2$-hybridized B atoms, $D_{3h}$-like geometry). (d) N K-edge NEXAFS spectrum of B-SSZ-13 in presence of template (solid black curve), of calcined B-SSZ-13 (dotted black curve), and after interaction with $NH_3$ at 373 K (solid gray curve). Residual pressure in the NEXAFS chamber: $10^{-9}$ mbar. All spectra have been recorded at liquid nitrogen temperature.

***Scheme 1.*** Pictorial Representation of the Effect of the Template Burning Process in B-SSZ-13, Where the $[B(OSi)_4]$ Units in a $T_d$-like Geometry ($sp^3$-Hybridized B Atoms) Are Transformed into $[B(OSi)_3]$ Units in a $D_{3h}$-like Geometry ($sp^2$-Hybridized B Atoms) upon Break of a B−O−Si Bond

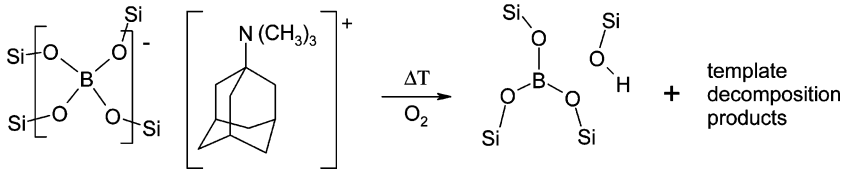


NEXAFS spectrum of calcined B-SSZ-13 like the broad components around 200 and 205 eV (appearing at 198 and 204 eV in $B_2O_3$ model compound; see Figure 1c). The band around 205 eV is assigned to the transition of B 1*s* electrons to the unoccupied B−O antibonding $\sigma^*$ orbital of $E'$ symmetry,[49] which is calculated to be ∼10 eV above the B $2p_z$ orbital.[53] However, the assignment of the peak at ∼200 eV is controversial in the literature. Tentatively it has been ascribed to the transition of B 1*s* electrons to empty B 3*p*,4*p* states on the basis of the weak Rydberg peaks in the XANES spectrum of gaseous $BF_3$.[51] Other fine features evident in the near-edge region of XANES may reflect either DOS structure or multiple scattering resonances. Summarizing, the NEXAFS curves reported in Figure 1a report features that match well, in a number of components and energy positions, with those of model compounds where B is in $sp^3$ (2 components) or in $sp^2$ (3 components) hybridization, respectively. Care must be taken when comparing the relative intensities of the different features. Fleet and Muthupari[48] have shown that the relative intensity of the different components may change significantly, even on the same sample, by changing the acquisition mode (e.g., by moving from total electron yield to fluorescence modes). Moreover note that model compounds contain a high density of B atoms, exhibiting thus other B atoms in their neighboring coordination shells. Owing to the low B content of B-SSZ-13 zeolite, B atoms are isolated, and this discrepancy may affect the relative intensities of the different XANES components.

The picture emerging from the here reported NEXAFS data perfectly matches the conclusions of the recent IR study by Regli et al.,[30] where it has been shown that the as-prepared B-SSZ-13 exhibits $[B(OSi)_4]$ units in a $T_d$-like geometry ($sp^3$-hybridized B atoms) while, upon template burning, the break of a B−O−Si bond results in $[B(OSi)_3]$ units in a $D_{3h}$-like geometry ($sp^2$-hybridized B atoms), testified by the appearance of the IR fingerprint at 1390 $cm^{-1}$, due to asymmetric B−O stretching.[54−56] Scheme 1 summarizes the model emerging from combined NEXAFS and IR results.

N K-edge NEXAFS spectra of B-SSZ-13 in the presence of the template is reported in Figure 1d as a solid black curve. In this case no normalization has been performed and the spectra are reported as they have been acquired. The spectrum is dominated by a huge component at 406.3 eV, with an evident high-energy tail around 413 eV. Two minor features appear at 398.6 and 400.8 eV, the intensities of which (referred to that

(53) Schwarz, W. H. E.; Mensching, L.; Hallmeier, K. H.; Szargan, R. *Chem. Phys.* **1983**, *82*, 57−65.
(54) Blaszczak, K.; Adamczyk, A.; Wedzikowska, M.; Rokita, M. *J. Mol. Struct.* **2004**, *704*, 275−279.
(55) Liu, H. B.; Shen, G. Q.; Wang, X. Q.; Wei, J. Z.; Shen, D. Z. *Prog. Cryst. Growth Charact. Mater.* **2000**, *40*, 235−241.
(56) Moon, O. M.; Kang, B. C.; Lee, S. B.; Boo, J. H. *Thin Solid Films* **2004**, *464−65*, 164−169.

***Scheme 2.*** Representation of the Nitridation Process Inside B-SSZ-13 Zeolite[a]

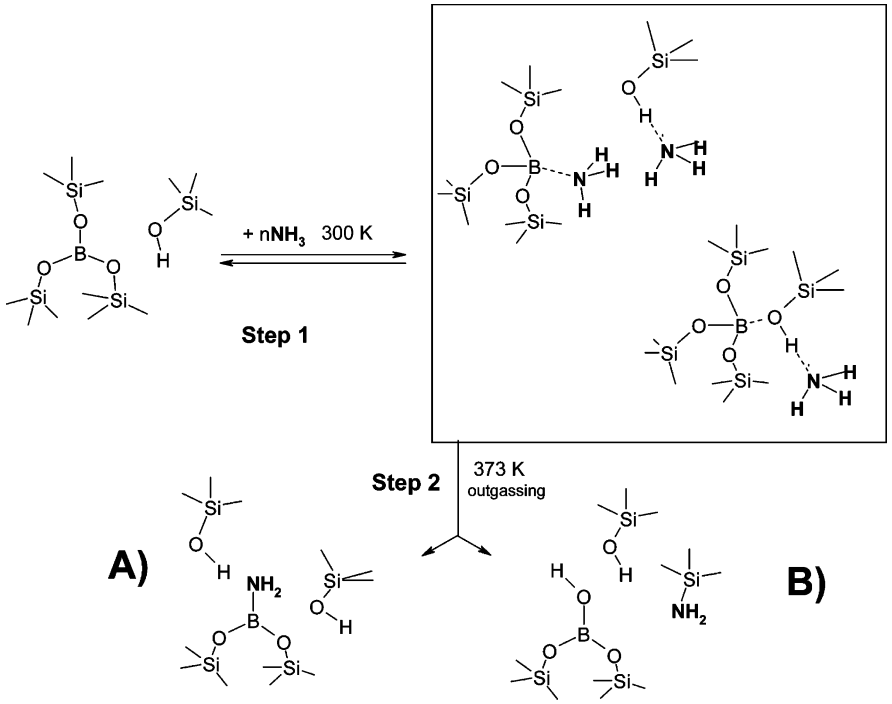


[a] Step 1: ammonia is adsorbed at room temperature. Step 2: heating up to 373 K results in the rupture of a B−O−Si bond with formation of a $-NH_2$ group either on boron (A) or on silicon (B).

of the dominant transition) are 0.05 and 0.04, respectively. The strong feature around 406 eV is traditionally assigned as a nitrogen $1s \rightarrow \sigma^*$ transition associated with N−H or N−C bonding.[57,58] In our case the component at 406.3 eV is associated to a $1s \rightarrow \sigma^*_{(N-C)}$ transition (see Scheme 1). The same work assigns a shakeup resonance to the shoulder around 412 eV in glycine,[57,58] a value that matches closely with our high-energy tail around 413 eV.

The minor features at lower energy fail in the spectral region where $1s \rightarrow \pi^*_{(N=C)}$ and $1s \rightarrow \pi^*_{N\equiv C)}$ transitions are expected. As the intensity of such bands increases with time in a set of spectra collected at room temperature (not reported), they are assigned to decomposition fragments of the template molecules. Note that a damaging effect of soft X-ray has been observed, e.g., for amino acids[59,60] or for nylon-6 or polyurethane[61] where the formation of N═C and N≡C bonds has been observed by N or C K-edge NEXAFS. As in the last spectrum collected at room temperature, the intensity of such components reaches values 15 times higher than that reported in Figure 1d (solid black curve); we consider the fraction of damaged template at liquid nitrogen temperature negligible.

No significant N K-edge signal was observed in the calcined sample (dotted spectrum in Figure 1d), testifying a virtually complete template removal.

**3.2. NEXAFS Study of B-SSZ-13 Nitridation upon Reaction with $NH_3$.** An NEXAFS study related to the interaction of the material with adsorbates is not straightforward, as the measurements have to be performed at a residual partial pressure not higher than $10^{-9}$ mbar. Of course this is a very strong limitation that avoids considering any ligand characterized by a weak bond with the zeolitic framework. For example water is removed from the coordination sphere of boron and the NEXAFS spectrum is virtually indistinguishable from that obtained for the calcined sample.

The B K-edge NEXAFS spectra of B-SSZ-13 after interaction with $NH_3$ is reported in Figure 1a, as a solid gray curve. This spectrum resembles closely that of the calcined zeolite (dotted curve), which suggests that $NH_3$ is totally removed from the zeolite at $10^{-9}$ mbar. This result is not unexpected as, e.g., CO, that is adsorbed on $Cu^+$ cations in zeolites with a $-\Delta_{ads}H$ as high as 130 kJ $mol^{-1}$,[62] is totally removed from the zeolite framework under UHV conditions of an XPS instrument.[63] This conclusion must however be revised on the basis of the N K-edge NEXAFS spectrum of B-SSZ-13 after interaction with $NH_3$ (Figure 1d, solid gray curve) where a remarkable signal, not present in the calcined sample, has been observed. This testifies that the interaction with ammonia at 373 K causes the insertion in the zeolitic framework of a significant fraction of nitrogen atoms that are stable under UHV conditions.

The N K-edge spectrum of B-SSZ-13 after interaction with $NH_3$ (solid gray curve) has been arbitrarily normalized in order to match the intensity of the 406 eV component with that of the same band measured in the as-prepared sample (solid black curve in the same figure). The spectrum is characterized by an intense and well structured band exhibiting three components at 398.6, 3.99.9, and 401.3 eV with a relative intensity with

(57) Gordon, M. L.; Cooper, G.; Morin, C.; Araki, T.; Turci, C. C.; Kaznatcheev, K.; Hitchcock, A. P. *J. Phys. Chem. A* **2003**, *107*, 6144−6159.
(58) Otero, E.; Urquhart, S. G. *J. Phys. Chem. A* **2006**, *110*, 12121−12128.
(59) Zubavichus, Y.; Zharnikov, M.; Shaporenko, A.; Fuchs, O.; Weinhardt, L.; Heske, C.; Umbach, E.; Denlinger, J. D.; Grunze, M. *J. Phys. Chem. A* **2004**, *108*, 4557−4565.
(60) Zubavichus, Y.; Fuchs, O.; Weinhardt, L.; Heske, C.; Umbach, E.; Denlinger, J. D.; Grunze, M. *Radiat. Res.* **2004**, *161*, 346−358.
(61) Coffey, T.; Urquhart, S. G.; Ade, H. *J. Electron Spectrosc. Relat. Phenom.* **2002**, *122*, 65−78.
(62) Bolis, V.; Barbaglia, A.; Bordiga, S.; Lamberti, C.; Zecchina, A. *J. Phys. Chem. B* **2004**, *108*, 9970−9983.
(63) Bolis, V.; Maggiorini, S.; Meda, L.; D'Acapito, F.; Palomino, G. T.; Bordiga, S.; Lamberti, C. *J. Chem. Phys.* **2000**, *113*, 9248−9261.

***Scheme 3.*** Representation of the Different Clusters Used To Simulate the B K-Edge NEXAFS Spectra of the Different B Species Foreseen in B-SSZ-13 after Reaction with $NH_3$ at 373 K

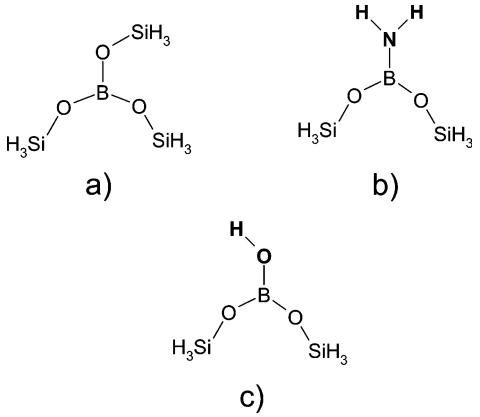


respect to the main band (here at 406.9 eV) of 0.84, 0.66, and 0.29, respectively. At higher energy the main band at 406.9 eV exhibits a shoulder around 411 eV. These features are typical of the NEXAFS spectra of $-NH_2$ species.[58]

In fact, clear differences can be observed in the nitrogen 1*s* spectra of species that contain the amine group ($-NH_2$, in a $C_{2v}$-like geometry) relative to species containing the protonated amine group ($-NH_3^+$ in a $C_{3v}$-like geometry). Specifically, a distinct low-energy band can be observed in species containing the $-NH_2$ groups.[58] In particular, this low-energy band, attributed to the $1s \rightarrow \sigma^*_{(N-H)}$ transition, has been observed at 402.5 eV in glycine sodium salt and at 402.3 eV in poly(allylamine).[58] These two model compounds also exhibit high-energy features: a band at 406.3 eV (406.2 eV) and a shoulder around 413−416 eV (415 eV) for glycine sodium salt (poly(allylamine). In summary, the overall spectrum of B-SSZ-13 after interaction with $NH_3$ (Figure 1d) is very similar to that of the model compounds described above, strongly suggesting the formation of stable $-NH_2$ groups inside the zeolite. An X-ray diffraction pattern of the reacted sample compared with the virgin one indicates that the thermal treatment in $NH_3$ has not affected the crystallinity; see Figure S1 of the Supporting Information.

The fact that we observe three components in the region of $1s \rightarrow \sigma^*_{(N-H)}$ transitions and a very broad component around 406 eV suggests the presence of heterogeneity in the $-NH_2$ species in the ammonia treated B-SSZ-13 sample. Once recognized that the $NH_3$ treatment has anchored $-NH_2$ species in the zeolitic framework, the observation of an unchanged B K-edge (Figure 1a) can be explained assuming a proton transfer from the $NH_3$ molecule to the zeolite framework, causing the rupture of one out of the three B−O−Si bridges and the formation of either $[O_2BOH]$ and $[H_2N-SiO_3]$ species or $[O_2BNH_2]$ and $[HO-SiO_3]$ species, according to step 2 in Scheme 2. Following this path, both $[O_2BOH]$ and $[O_2BNH_2]$ species, exhibiting a trigonal planar geometry, are expected to keep the 194.4 eV component in the B K-edge NEXAFS spectrum.

Further information on the nature of the $-NH_2$ species stable at $10^{-9}$ mbar comes from IR spectra (section 3.3) and ab initio calculations (section 3.4), confirming that a nitridation of the zeolitic framework occurred upon very mild treatment.

**3.3. Simulation of NEXAFS Spectra.** Different approaches are used to calculate X-ray absorption near edge structures. The most diffuse one use the local density approximation to calculate the final state. This is done considering infinite crystals, adopting a band structure approach,[64] or clusters using the multiple scattering theory.[65,66] Typically, multiple scattering theories employ an important approximation: the muffin-tin averaging of the potential needed for the expansion of the wave functions.

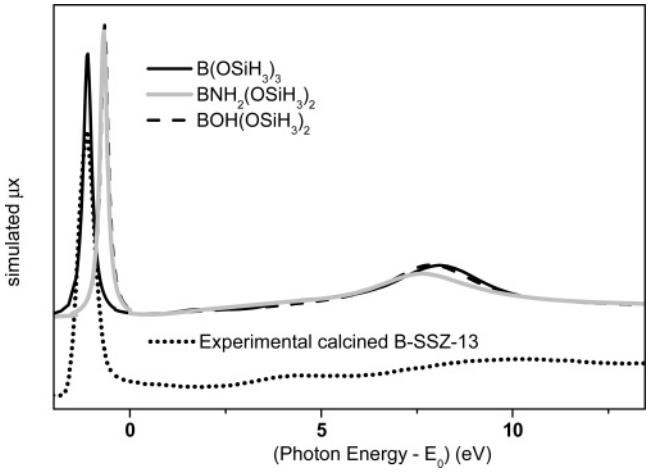


***Figure 2.*** Simulated B K-edge NEXAFS spectra computed applying the FDMNES code[70] on the clusters reported in Scheme 3. For comparison the experimental spectrum of the calcined B-SSZ-13 zeolite (gray curve) has been superimposed by arbitrarily matching the position and the intensity of its first resonance with that of the $[B(OSiH_3)_3]$ cluster.

This approximation is serious, especially when the photoelectron kinetic energy is close to the value of the approximation done on the potential, and moreover, it makes the results depend on the size of the interstitial region between the muffin-tin spheres. To avoid the restriction imposed by this approximation several computing methods have been developed and successfully applied.[67−70] Between them the finite difference method currently included in the FDMNES code emerges as providing more reliable results and greater algorithmic stability.[70] This method has been used in this work to simulate the NEXAFS of B atoms in B-SSZ-13. The clusters used for the simulation are shown in Scheme 3. The tridimensional coordinate of B, O, N, and Si has been taken from the quantum mechanical calculation described later (section 3.5), while the H atoms have been optimized by the DMol$^3$ code developed inside the accelrys frame.[71−73]

According to the reaction mechanisms described in Scheme 2, three different families of B atoms can exist inside the B-SSZ-13 framework: unreacted $[B(OSi)_3]$ units, $[H_2NB(OSi)_2]$ or $[HOB(OSi)_2]$ products depending on whether path A or B of Scheme 2 has been followed. Scheme 3 reports the clusters adopted to compute the simulated NEXAFS spectra for the three

(64) Mattheiss, L. F.; Dietz, R. E. *Phys. Rev. B* **1980**, *22*, 1663−1676.
(65) Rehr, J. J.; Albers, R. C.; Zabinsky, S. I. *Phys. Rev. Lett.* **1992**, *69*, 3397−3400.
(66) Tyson, T. A.; Hodgson, K. O.; Natoli, C. R.; Benfatto, M. *Phys. Rev. B* **1992**, *46*, 5997−6019.
(67) Ahlers, D.; Schutz, G.; Popescu, V.; Ebert, H. *J. Appl. Phys.* **1998**, *83*, 7082−7084.
(68) Ahlers, D.; Attenkofer, K.; Schutz, G. *J. Appl. Phys.* **1998**, *83*, 7085−7087.
(69) Huhne, T.; Ebert, H. *Solid State Commun.* **1999**, *109*, 577−582.
(70) Joly, Y. *Phys. Rev. B* **2001**, *63*, 125120 (http://125147.125173.125148.125195/LDC/LE_LABORATOIRE/Equipes_de_recherche/EQUIPE_SPECTROSCOPIE/SIMUL/EtudFond_Prog.asp).
(71) Delley, B. *J. Chem. Phys.* **1990**, *92*, 508−517.
(72) Delley, B. *J. Phys. Chem.* **1996**, *100*, 6107−6110.
(73) Delley, B. http://www.accelrys.com/mstudio/dmol3.html.

above-mentioned B species. Note that all species concern $sp^2$-hybridized B atoms having a first coordination shell in a $D_{3h}$-like geometry. This holds in the first approximation also for the $[H_2NB(OSi)_2]$ species (Scheme 3b) owing to the almost indistinguishable electron scattering power of N and O atoms.

The simulated spectra reported in Figure 2 are able to reproduce the three main experimental features observed experimentally for $sp^2$-hybridized B in a $D_{3h}$-like geometry and deeply discussed in section 3.1: in detail, a sharp component just below $E_0$, a weak and well-defined component in the $(E - E_0)$ region around 2−5 eV, and a stronger and broad component in the $(E - E_0)$ region around 6−10 eV. When comparison with the experimental spectrum is done, the agreement in the relative energy position and relative intensity of these three features is satisfactory.

Comparing the computed spectra, the sharp feature below $E_0$ undergoes a blue shift of about 0.5 eV and a very small intensity increase (less than 10%) by moving from $[B(OSiH_3)_3]$ to $[H_2NB(OSiH_3)_2]$ or $[HOB(OSi\ H_3)_2]$ clusters. As for the other minor two components, they are almost indistinguishable in three simulated clusters. From the here reported simulations it is impossible to discriminate between $[H_2NB(OSiH_3)_2]$ and $[HOB(OSiH_3)_2]$ clusters. The fact that the three clusters have an NEXAFS spectrum dominated by the sharp component just below $E_0$ reflects their $D_{3h}$-like geometry; this observation confirms the fingerprint nature of this band for $sp^2$-hybridized B in planar $D_{3h}$ geometry.

According to our simulations, the difference in the NEXAFS spectra of unreacted (Scheme 3 a and full black curve in Figure 2) and of reacted (Scheme 2b,c and solid gray and dashed black curves in Figure 2) B species basically consists only of a small (0.5 eV) shift of the $D_{3h}$-like-fingerprint band. As this band, in the experimental spectrum, has an FWHM (0.5 eV) that is twice that of the simulated ones, it is evident that NEXAFS spectroscopy can differentiate the calcined B-SSZ-13 sample from the nitridized one only assuming that almost all B species have reacted with ammonia. Actually, the experimental B K-edge NEXAFS spectrum of the nitridized B-SSZ-13 zeolite can be reasonably hypothesized as the superimposition of NEXAFS spectra coming from the three different families of B species depicted in Scheme 3. From IR data (vide infra inset in Figure 3c) we estimate that about 50% of the B atoms have reacted according to Scheme 2. The fact that the three families of B sites (Scheme 3) are expected to have very similar NEXAFS features (Figure 2) and the fact that almost 50% of the B sites have not reacted can explain why we did not observe significant differences between the experimental NEXAFS spectra before and after $NH_3$ treatment (Figure 1a).

**3.4. Nitridation of B-SSZ-13 Followed by IR Spectroscopy.** The IR spectrum of an activated B-SSZ-13 is characterized by a complex spectrum in the OH stretching region: silanol bands at 3745 $cm^{-1}$ (shoulder) and a doublet at 3733 and at 3715 $cm^{-1}$ (black curve in Figure 3a). These features, by analogy with what already was observed for H-SAPO-34 and for H-SSZ-13,[74−76] labeled as HF and LF components, have been assigned to Brønsted sites characterized by a very weak acidity, being

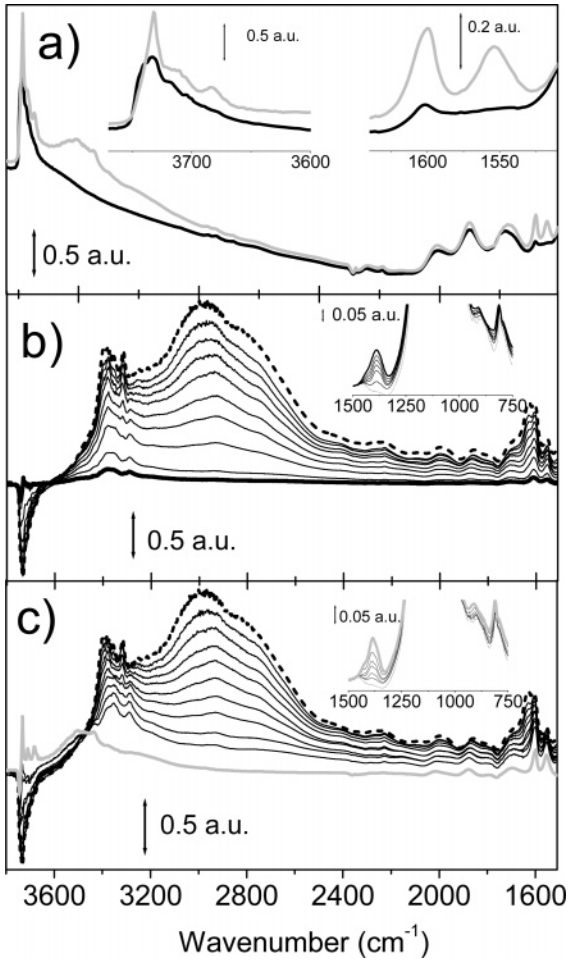


***Figure 3.*** (a) IR spectra of B-SSZ-13 zeolite activated at 773 K in vacuo (black curve) and after interaction at 373 K with 35 mbar of $NH_3$ and successive outgassing down to $10^{-3}$ mbar (gray curve). The left and right insets report a magnification of the O−H and N−$H_2$ stretching regions, respectively. (b) IR spectra of increasing doses of $NH_3$, up to 35 mbar (bold curve) on a B-SSZ-13 sample activated at 773 K in vacuo. Main part: background subtracted spectra collected on a self-supported pellet. Inset: spectra collected on a thin film deposited on a silicon wafer. (c) Same as part (a) for the room temperature desorption experiment starting from $NH_3$ equilibrium pressure of 35 mbar (bold curve) down to $10^{-3}$ mbar. Gray bold curve: IR background subtracted spectrum collected after outgassing the system at 373 K, corresponding to the gray spectrum in part (a). a.u. = absorbance units. Figure S3 of the Supporting Information reports the spectra of parts (b) and (c) without background subtraction.

associated with B(OH)Si groups.[30] These species readily interact with $NH_3$ as testified by the spectra reported in Figure 3.

Figure 3a reports IR spectra of a B-SSZ-13 zeolite activated at 773 K in vacuo (black curve) and after interaction at 373 K with 35 mbar of $NH_3$ and successive outgassing down to $10^{-3}$ mbar (gray curve). The spectra reported in the main parts of Figure 3b,c are background subtracted and are related to $NH_3$ in interaction with a compressed self-supported zeolite wafer. Parts (b) and (c) correspond to adsorption and desorption experiments, respectively. Conversely, in the corresponding insets, the results of a parallel experiment performed on a thin layer of B-SSZ-13 deposed on a silicon wafer are reported.

Increasing doses of $NH_3$ generate the progressive erosion of the original $\nu$(OH) bands and the parallel formation of a large complex absorption extended in the 3600−2000 $cm^{-1}$ range (Figure 3b). The main absorption in the 3400−2000 $cm^{-1}$ range is due to hydroxyl groups perturbed by $NH_3$ and forming

(74) Frache, A.; Gianotti, E.; Marchese, L. *Catal. Today* **2003**, *77*, 371−384.
(75) Bordiga, S.; Regli, L.; Cocina, D.; Lamberti, C.; Bjorgen, M.; Lillerud, K. P. *J. Phys. Chem. B* **2005**, *109*, 2779−2784.
(76) Martins, G. A. V.; Berlier, G.; Coluccia, S.; Pastore, H. O.; Superti, G. B.; Gatti, G.; Marchese, L. *J. Phys. Chem. C* **2007**, *111*, 330−339.

hydrogen bonds of medium strengths. Three main contributions, recognized at about 3010, 2930, and 2760 $cm^{-1}$, can be associated with perturbed silanol, LF, and HF groups, respectively.[77,78] At higher frequency, a group of bands associated with ammonia modes are present. In particular, at low pressure of ammonia, a broad component centered at 3380 $cm^{-1}$ and a band at 3288 $cm^{-1}$, due to $\nu(N-H)_{asym}$ and $\nu(N-H)_{sym}$ modes of adsorbed $NH_3$, grow. When $NH_3$ coverage is increased, the appearance of a sharp peak at 3316 $cm^{-1}$ and the modification of previous bands testify the formation of $NH_3$ adlayers. In the range 2100−1600 $cm^{-1}$, where the overtones of framework vibrations occur, we observe weak "false" bands (derivative-type) which are generated through the spectra subtraction.[79,80] This happens because framework modes are slightly shifted in the presence of adsorbates condensed in the pores. At 1610 $cm^{-1}$ and at 1555 $cm^{-1}$ we observe the appearance of a doublet that increases in intensity upon $NH_3$ adsorption. These spectroscopic features are the consequences of the formation of $[SiO]_3B\cdots NH_3$ (1610 $cm^{-1}$) and $[SiO]_3Si-OH\cdots NH_3$ (1555 $cm^{-1}$) adducts[43] as depicted in step 1 of Scheme 2. At higher $NH_3$ coverages, the band at 1630 $cm^{-1}$, due to the bending mode of physisorbed ammonia, shows up testifying the incoming growth of a condensed phase inside the pores.

In the inset of part (b) of Figure 3, the effect of increasing doses of ammonia on skeletal vibration modes that involve boron atoms is reported. The decrease in intensity occurs until the complete disappearance of the band at 1390 $cm^{-1}$ is observed, while the band at about 912 $cm^{-1}$ (due to Si−O modes perturbed by the presence of boron) undergoes a shift at lower frequency. This behavior is similar to what was observed upon dosing $H_2O$ or $CH_3OH$ on the same material.[30] These results can be explained in terms of a change in boron site coordination that moves from a $D_{3h}$ symmetry to a distorted tetrahedral one (see structures reported in the box of Scheme 2). It is important to underline that from the boron coordination point of view; both of the situations depicted in the box of Scheme 2 ($NH_3$ directly bonded to boron and $NH_3$ interacting with the silanol in the first coordination sphere of boron) should have a very similar spectroscopic effect.

The interaction with $NH_3$ is not completely reversible at room temperature as it is documented in part (c) of Figure 3 where, upon decreasing $NH_3$ equilibrium pressure, the intensity of the bands associated to physisorbed ammonia is reduced progressively (peaks at 3316 and 1630 $cm^{-1}$), but the original spectrum is not recovered. In particular, in the OH stretching region we observe the partial restoration of the three components associated to silanols (3745 $cm^{-1}$ (shoulder) and a doublet at 3733 and 3715 $cm^{-1}$) and the parallel erosion of the broad band extended until 2000 $cm^{-1}$, due to $[SiO]_3Si-OH$ groups interacting with ammonia. In the meantime, the bands due to $\nu$(NH) (3380 and 3288 $cm^{-1}$) and $\delta$(NH) (1610 and 1555 $cm^{-1}$) modes, although reduced, are still present. Finally, it is interesting to observe that both the $\nu$(B−O) stretching mode related to the $[BO_3]$ unit and the $\nu$(Si−O) mode perturbed by the presence of boron are not completely restored (see inset of Figure 3c). The spectra evolution suggests that a prolonged outgassing at room temperature produces the elimination of most of the physisorbed ammonia, while $NH_3$ molecules are still in direct interaction with specific $[SiO]_3B$ sites and with a fraction of the $[SiO]_3Si-OH$ silanols.

B-SSZ-13 sample in the presence of the irreversible fraction of $NH_3$ has been heated at 373 K and then subjected to a further desorption down to $10^{-3}$ mbar (gray curve in Figure 3c). The broad absorption extended in the 3200−2000 $cm^{-1}$ range and the bands at 3380 and 3288 $cm^{-1}$ are completely removed, testifying the complete removal of adsorbed ammonia. Moreover this moderate thermal treatment causes the formation of new components that can be only explained in term of a reaction between $NH_3$ and the zeolite. In particular we observe the following: (*i*) the formation of new OH groups (narrow bands at 3730, 3710, and 3680 $cm^{-1}$); (*ii*) most importantly, the formation of a broad absorption where two complex bands with maxima at 3430 and 3500 $cm^{-1}$ are recognizable. These species are easily ascribed to the stretching modes of $-NH_2$ groups, as they appear at a higher frequency than the $\nu$(N−H) in ammonia. The formation of $-NH_2$ species anchored to the zeolitic framework is confirmed by the clear permanence of a doublet (1600 and 1550 $cm^{-1}$) in the $\delta(NH_2)$ region[22,25,28,58,81] that could be associated with two different $-NH_2$ species: $B-NH_2$ and $Si-NH_2$, formed upon rupture of a B−O−Si framework bond. Further comments on these species will be given on the basis of *ab initio* modeling results (section 3.5). All these IR features fully support the conclusions drawn on the basis of our NEXAFS study and summarized in the reaction paths reported in Scheme 2 parts A and B of step 2. The observation that a gentle thermal treatment (373 K) has been able to produce the formation of $-NH_2$ species bonded directly to boron or to silicon is of relevance, as all attempts to functionalize microporous and mesoporous silicates with $-NH_2$ groups described so far require very long treatments at high temperature.[21,22,25]

From this set of data, it is determined that the insertion of boron inside the zeolite confers peculiar properties that allow an easy functionalization of the surface. A similar behavior has been observed also in the case of interaction with methanol where an extensive and stable methoxylation has been observed upon interaction with methanol, already at room temperature.[30]

**3.5. Reactivity of B−O−Si Bonds toward $NH_3$: Ab Initio Study of the Energetic and Vibrational Properties.** Ab initio B3LYP/6-31+G(d,p) calculations were carried out on cage cluster models; see Figure 4 for the optimized structures. Cage clusters have been successfully adopted in the past to mimic acidic active sites in silica and silico-alumina materials of both amorphous and microporous crystalline nature[42−46] and to simulate the reactivity of heteroatoms like Ti.[47] In this case we have used the $Si_7BO_{12}H_7$ cage envisaging 6 four-member rings with seven tetrahedral Si and one trigonal B atoms (see cluster *Cage* in Figure 4). Even if no symmetry constraints have been imposed, the local geometry around B is almost $D_{3h}$, with three equivalent B−O bonds at 1.37 Å. Considering that the average Si−O bond length is around 1.65 Å, the introduction of B causes a relevant strain in the structure. The *Cage* cluster, although relatively simple, is able to reproduce the IR fingerprint of

(77) Zecchina, A.; Marchese, L.; Bordiga, S.; Paze, C.; Gianotti, E. *J. Phys. Chem. B* **1997**, *101*, 10128−10135.
(78) Koller, H.; Fild, C.; Lobo, R. F. *Microporous Mesoporous Mater.* **2005**, *79*, 215−224.
(79) Zecchina, A.; Geobaldo, F.; Spoto, G.; Bordiga, S.; Ricchiardi, G.; Buzzoni, R.; Petrini, G. *J. Phys. Chem.* **1996**, *100*, 16584−16599.
(80) Paze, C.; Bordiga, S.; Lamberti, C.; Salvalaggio, M.; Zecchina, A.; Bellussi, G. *J. Phys. Chem. B* **1997**, *101*, 4740−4751.
(81) Kaskel, S.; Farrusseng, D.; Schlichte, K. *Chem. Commun.* **2000**, 2481−2482.

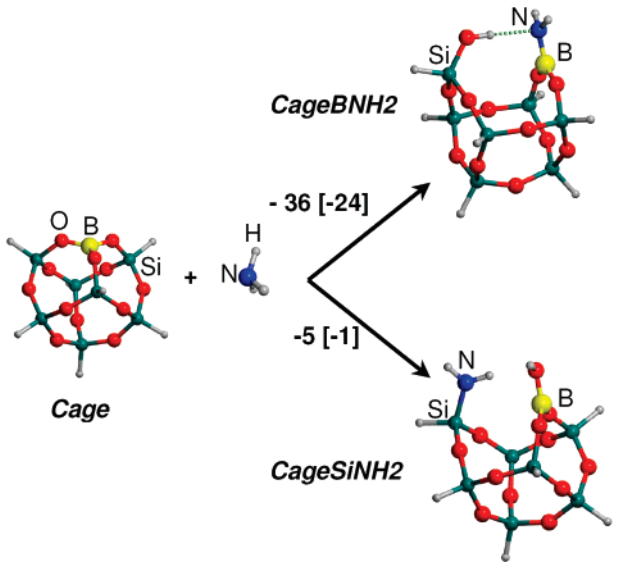


***Figure 4.*** Optimized geometries for the *Cage* cluster modeled adopted to simulate the two possible reaction paths of $NH_3$ with a B-zeolite at the ab initio B3LYP/6-31+G(d,p) level: *Cage* + *NH3* → *CageBNH2* (Scheme 2A) and *Cage* + *NH3* → *CageSiNH2* (Scheme 2B). Also reported is the relative stability in kJ/mol computed at the B3LYP/6-31+G(D,P) level and at the MP2 level, in square brackets. For a comparison of the computed and experimental frequency shifts [$\Delta\nu(NH)_{asym}$, $\Delta\nu(NH)_{sym}$, $\Delta\delta(NH_2)$, and $\Delta\nu(OH)$], see Table 1.

B-zeolites, found experimentally at 1390 $cm^{-1}$ as an asymmetric stretching of the [$BO_3$] unit computed at 1355 $cm^{-1}$.

Upon reaction with ammonia two different products are expected, as already shown in Scheme 2, namely clusters *CageBNH2* and *CageSiNH2* in Figure 4. In the former, ammonia reacts forming an $NH_2$ group attached to the B and an adjacent silanol; in the latter, the reverse happens.

Please note that for the *CageBNH2* cluster the formed silanol enjoys a H-bond with the $NH_2$ group (see dashed line). This fact testifies the basic character of such B−$NH_2$ groups. As expected, although not imposed, the local geometry around B is $D_{3h}$-like in agreement with the NEXAFS and IR spectra collected on the calcined B-SSZ-13 sample both before and after reaction with $NH_3$. Both reactions are energetically favored, although the formation of *CageSiNH2* cluster is definitely less favored (−5 vs −36 kJ/mol at the B3LYP/6-31+G(D,P) level). MP2/6-311++G(2p,2d) single-point energy calculation using optimized B3LYP/6-31+G(D,P) geometries does not change the relative stability, despite results in less pronounced energy minima (−1 and −24 kJ/mol for *CageSiNH2* and *CageBNH2* clusters, respectively). A fraction of the stability of the *CageBNH2* cluster is due to the internal H-bond, which occurs naturally upon rupture of a B−O−Si bridge by ammonia according to Scheme 2A. The same does not occur when $NH_2$ is attached to Si because the B−OH unit remains in the [$BO_3$] plane. The contribution of the H-bond to the stability of the *CageBNH2* cluster has been estimated by constraining the Si−OH group to point away from the B−$NH_2$ group. The reaction energy obtained using the constrained cluster (*CageSiNH2** in Figure S4 of the Supporting Information) is reduced to −24 [−17] kJ/mol at the B3LYP/6-31+G(D,P) [MP2] level, suggesting an H-bond strength of about 10 kJ/mol. On the basis of the here reported calculations the formation of B−$NH_2$ species (Scheme 2A) seems highly favored with respect to Si−$NH_2$ species (Scheme 2B). However, as H-bonds account for about

***Table 1.*** Comparison between Experimental Frequency Shifts [from Gray Bold Spectrum in Figure 3b] and B3LYP/6-31+G(d,p) Unscaled Harmonic Frequencies [from Eqs 1,2]

| | $NH_2$ spectral region | | |
|---|---|---|---|
| | *CageSiNH2* | *CageBNH2* | experiment ($cm^{-1}$) |
| $\Delta\nu(NH)_{asym}$ | +64 | +75 | +56/+96 |
| $\Delta\nu(NH)_{sym}$ | +108 | +115 | +93/+128 |
| $\Delta\delta(NH_2)$ | −86 | −50 | −27, −77 |

30% of the overall energy of the *CBNH2* cluster, the presence of additional H-bond interactions between the B−OH group of the *CageSiNH2* cluster, and a proximal framework Si−OH group, not foreseen in the models adopted in this study could further stabilize the product envisaging Si−$NH_2$ species. Note that a vicinal Si−OH group is needed to ensure the electrical neutrality of the framework (see first part of Scheme 2). This fact hampers any attempt to derive a quantitative estimate of the relative population of the two products, so that we consider both in the following for the interpretation of the IR spectrum.

The B3LYP/6-31+G(d,p) spectroscopic features have been compared to the experimental ones to contribute in the interpretation of experimental absorptions. Because computed IR modes do not include anharmonicity, only frequency shifts $\Delta\nu$ have been considered, computed as the differences between the modes of the −$NH_2$ surface species (*CageSiNH2* and *CageBNH2* models, named $\nu(NH)_{surf}$ and $\delta(NH_2)_{surf}$) and the corresponding B3LYP/6-31+G(d,p) modes for the free $NH_3$ molecule (named $\nu(NH)_{NH3\ and}$ $\delta(NH_2)_{NH3}$), according to eqs 1 and 2:

$$\Delta\nu(NH) = \nu(NH)_{surf} - \nu(NH)_{NH_3} \quad (1)$$

$$\Delta\delta(NH_2) = \delta(NH_2)_{surf} - \delta(NH_2)_{NH_3} \quad (2)$$

The experimental frequency shifts ($\Delta\nu(NH)_{asym}$, $\Delta\nu(NH)_{sym}$, $\Delta\delta$-$(NH_2)$) reported in Table 1 have been worked out as the differences between the bands attributed to the −$NH_2$ modes of the nitridated sample, gray bold curve, Figure 3c) and the corresponding experimental modes of gas-phase $NH_3$.[82]

Due to the complexity of the experimental features observed in the $\nu(NH)$ stretching region, $\Delta\nu$ values are given in an interval ($\Delta\nu(NH)_{asym}$ = +56/+96 $cm^{-1}$ and $\Delta\nu(NH)_{sym}$ = +93/+128 $cm^{-1}$, respectively). The computed shifts for the two models (*CageSiNH2* and *CageSiNH2*) are similar and in qualitative agreement with the features observed experimentally. Note that for both $\nu(NH)_{asym}$ and $\nu(NH)_{sym}$ larger shifts have been computed for −B−$NH_2$ species. Coming to the bending modes, the experimental doublet at 1600 and 1550 $cm^{-1}$ ($\Delta\delta(NH_2)$ = −27 and −77 $cm^{-1}$, respectively) can be due to the contemporary presence of −B−$NH_2$ (computed $\Delta\delta(NH_2) = -50\ cm^{-1}$) and −Si−$NH_2$ species (computed $\Delta\delta(NH_2) = -86\ cm^{-1}$). This relatively good agreement between computed and experimental IR features supports the copresence of both species.

To explain the IR doublet in the $\delta(NH_2)$ region both −B−$NH_2$ and −Si−$NH_2$ species are needed, as shown above. Whereas the −B−$NH_2$ species can be formed on B-containing zeolites only, the −Si−$NH_2$ species can (at least in principle)

(82) Shimanouchi, T. Molecular Vibrational Frequencies. In *NIST Chemistry WebBook*; NIST Standard Reference Database Number 69, 20899 (http://webbook.nist.gov); Linstrom, P. J., Mallard, W. G., Eds.; National Institute of Standards and Technology: Gaithersburg, MD, 2005.


***Figure 5.*** Optimized geometries for the $[Si_8O_{13}H_8]$ cluster model adopted to simulate the possible nitridation reaction path of a surface silanol on a purely silicelous material. Also reported is the reaction energy in kJ/mol computed at the B3LYP/6-31+G(D,P) level.

derive from a reaction of $NH_3$ with terminal Si−OH groups at the crystal surface with water elimination. However this reactivity under such mild conditions has never been observed neither on silica nor on zeolites. The cage cluster model adopted so far is able to reproduce this experimental evidence. Figure 5 reports the optimized structures for an isolated surface silanol, $Si_8O_{13}H_8$ cluster, reacting with ammonia to give the $Si_8O_{12}$-$NH_9$ cluster plus water. The simulated reaction is endothermic by 45 kJ/mol at the B3LYP/6-31+G(D,P) level.

The unreactivity of the silica surface Si−OH groups toward ammonia, correctly reproduced by the computational results reported in Figure 5, combined with the reactivity of B-containing frameworks, foreseen by the analogous computations summarized in Figure 4, underlines the fundamental role played by framework B species in the possibility of inserting $NH_2$ groups inside zeolitic frameworks under mild treatment conditions.

## 4. Conclusions and Future Perspectives

We have reported clear evidence of the formation of $B-NH_2$ (dominant species) and $Si-NH_2$ (minority species) surface functionality inside the pores of B-SSZ-13 zeolite contacted with 35 mbar of $NH_3$ at 373 K for 30 min. IR spectroscopy highlights the presence of two doublets at 3430 and 3500 $cm^{-1}$ and at 1600 and 1550 $cm^{-1}$ due to the stretching and bending modes of two different $-NH_2$ groups.[22,25,58,81] Such species are highly stable as they are persistent in the UHV condition ($10^{-9}$ mbar) of the NEXAFS chamber resulting in components in the 398−402 eV and 407−411 eV ranges of the NEXAFS spectra, regions where $-NH_2$ species are expected to contribute.[58] *Ab initio* B3LYP/6-31+G(d,p) calculations, refined at the MP2 level, shows that both reaction paths

$$(SiO)_2B-O-Si(OSi)_3 + NH_3 \rightarrow (SiO)_2B-NH_2 + H-O-Si(OSi)_3 \quad (3)$$

$$(SiO)_2B-O-Si(OSi)_3 + NH_3 \rightarrow (SiO)_2B-OH + H_2N-Si(OSi)_3 \quad (4)$$

are exothermic, reaction 3 being strongly favored. Despite this fact, we cannot exclude species $H_2N-Si(OSi)_3$ to be appreciably present because interactions with framework silanols, not accounted for by the adopted models, possibly acting as further stabilizing agents. For this reason models of both $(SiO)_2B-NH_2$ and $H_2N-Si(OSi)_3$ species have been used to assign experimental bands reaching a semiquantitative agreement.

The reactivity under such mild conditions toward ammonia is very peculiar for this system and has never been observed in pure siliceous and/or Al containing zeolites. The same cage cluster, when purely siliceous cannot react with ammonia, in agreement with experimental evidence. The presence of B atoms in the zeolitic framework is thus essential for the formation of framework $-NH_2$ groups. This behavior of framework B is tentatively explained by two factors. First the ability of $[B(OSi)_4]$ units in $T_d$-like geometry ($sp^3$-hybridized B atoms) to be transformed, upon template burning, into $[B(OSi)_3]$ units in $D_{3h}$-like geometry ($sp^2$-hybridized B atoms) with a break of a B−O−Si bond, results in the formation of Lewis acid centers able to specifically coordinate bases like $NH_3$. Second, the much smaller ionic radius of B(III), with respect to Si(IV) or Al(III), implies that a strain is contained in the $[B(OSi)_3]$ units when embedded in the zedolitic framework rigidity. This strain favors the break of another B−O−Si bond, significantly increasing the efficiency of reaction 3 or 4.

As the anchoring of $-NH_2$ species occurs in the presence of boron, the Si/B ratio 11 of our material implies that the maximum loading of the $-NH_2$ surface functionality inside the pores of B-SSZ-13 is 2.3 wt %, when all B atoms will react according to eq 3 or 4. From IR data on the relative intensity of the mode of trigonal B before and after heating at 373 K (see inset in Figure 3c) we estimate that we have reached about 50% of the hypothetical upper limit. We believe that this fraction can be improved by working at higher $NH_3$ equilibrium pressures. Note that the heating process has been performed on the sample evacuated at room temperature, thus containing only specifically adsorbed $NH_3$ molecules. This strategy allows the collection of high quality IR spectra able to testify to the formation of $-NH_2$ species, which is the aim of this first contribution. These findings can open a new route in the preparation of shape selective solid basic catalysts.

**Acknowledgment.** B-SSZ-13 samples used in this study have been synthesized in the Chevron Texaco Energy Research and Technology laboratories (Richmond, CA 94802) by Mr. Lun Teh Yuen. We are grateful to Dr. Stacey I. Zones for having kindly supplied us the material, for his continuous encouragements, and for the fruitful and friendly discussions. We are strongly indebted to Prof. F. Boscherini for a critical discussion of the whole set of experimental data and for having provided us the NEXAFS spectra of the model compounds reported in Figure 1b,c. The whole staff of the BEAR beamline at the Elettra synchrotron (in particular Dr. B. Doyle) are gratefully acknowledged for the important support during the NEXAFS data collection. This work has been partially supported by Compagnia di San Paolo (http://www.compagnia.torino.it/) funds.

**Supporting Information Available:** Complete ref 41; XRD patterns collected before and after treatment with $NH_3$; as-measured IR spectra (not difference) before and after $NH_3$ treatment; and the optimized geometry of the *CageSiNH2* cluster, obtained by constraining the Si−OH group to point away from the $B-NH_2$ group. This material is available free of charge via the Internet at http://pubs.acs.org.

JA0721770